Journal of Low Temperature Physics, Vol. 135, Nos. 3/4, May 2004 (© 2004)

Measurements of Attenuation of Third Sound: Evidence of Trapped Vorticity in Thick Films of Superfluid ^{4}He

J. A. Hoffmann,[1,2] K. Penanen,[3] J. C. Davis,[2] and R. E. Packard[1]

[1] *Physics Department, University of California at Berkeley, Berkeley, California 94720, U.S.A.*
E-mail: joaner@socrates.berkeley.edu
[2] *LASSP, Physics Department, Cornell University, Ithaca, New York 14853, U.S.A.*
[3] *Jet Propulsion Laboratory, California Institute of Technology, Pasadena, California 91109, U.S.A.*

(Received August 24, 2003; revised January 26, 2004)

We present results of a study of third sound in thick ^{4}He films in circular resonator geometry. Frequency and line shapes of third sound resonances are measured for temperatures between 0.3 and 2.1 K in saturated films approximately 30 nm thick. From these measurements we calculate the attenuation of the sound. We find that the attenuation at a given temperature is a function of history of the film, strongly affected by such events as large, sudden (more than milli-Kelvin per second) temperature spikes. We also observe variable frequency splitting of resonances, indicating trapped circulation. Our measurements, taken together with other reported attenuation experiments, are incompatible with dissipation mechanisms dependent on thermodynamic properties alone. Measurements indicate a linear dissipation mechanism, inconsistent with vortex drag and re-connection models. We conclude that high attenuation values, evidence of trapped circulation, and variation in attenuation values support the hypothesis that thick films of ^{4}He contain high densities of remnant quantized vortices. The vortex populations suggested by trapped circulation are consistent with proposed linear dissipation mechanisms due to vortex-normal fluid interactions and vortex dimple drag.

***KEY WORDS*:** third sound; helium film; quantized vortices.

1. MOTIVATION

Third sound has proven to be a powerful probe of helium films, observed first in ^{4}He in 1962[1] and subsequently used to study various film properties.[2–6] It has also been observed in ^{3}He films.[7] Other studies have probed properties of ^{3}He-^{4}He mixtures in thin films.[8,9]

0022-2291/04/0500-0177/0 © 2004 Plenum Publishing Corporation

Previous attempts[10–12] to describe third sound in ^{4}He films use a hydrodynamic approach, treating the superfluid as homogeneous and defect-free. This approach leads to a good understanding of the propagation speed, but has not been successful in explaining the attenuation α. Hydrodynamic calculations for attenuation in a homogeneous superfluid give predictions much smaller than those experimentally observed, especially in thick films. The few published results of attenuation measurements for thick films indicate dependence on both history and surface preparation. For example, in the earliest work[2] attenuation measurements taken in the same experimental cell in two subsequent runs varied by as much as factor of two. Attempts to explain the high dissipation involve mechanisms which include a macroscopic uncertainty principle[13] or interactions with trapped (remnant) vorticity. Ellis suggests that remnant vortices may be dragged along the surface of the film.[6]

Here we revisit the question of third sound attenuation, bearing in mind the inconsistencies reported in previous work. We look especially for indications of remnant vorticity, as recent theoretical proposals[6, 14] suggest that dissipation due to vortices may be the dominant mechanism of attenuation. These indications would include history dependent behavior and sensitivity to events known to influence vortex creation/pinning, such as temperature gradient driven critical film flow.

2. INTRODUCTION

The two-fluid model of superfluidity describes ^{4}He below the superfluid transition temperature $T_\lambda \approx 2.17$ K as comprising two interpenetrating fluids, normal and superfluid, each with its own density ρ and velocity field $\vec{v}$. The total density and mass current density are expressed as the sum of the components

$$\rho = \rho_n + \rho_s \tag{1}$$

$$\vec{J} = \rho_n \vec{v}_n + \rho_s \vec{v}_s, \tag{2}$$

where the subscripts n and s designate normal and superfluid components, respectively. Atkins noted in 1959 that if the spatial extent of the helium is less than the viscous penetration depth, this description allows for hydrodynamic modes in which the normal fluid component is clamped and only the superfluid component, with no viscosity, is in motion.[10] This condition is satisfied when the system is confined either to a film on a substrate (which allows for surface waves, called third sound) or to a porous medium (fourth sound). In this work, the lower bound for the viscous penetration

depth, corresponding to $\omega \approx 2\pi \cdot 60$ Hz, $\rho_n(T) \approx \rho_n(2.1\ \mathrm{K})$ is calculated to be $\delta = \sqrt{\frac{2\eta}{\omega \rho_n}} = 30\ \mu\mathrm{m}$ and is a weak function of temperature. This length is three orders of magnitude greater than the maximum thickness of films studied in the present work.

The speed of a wave in a shallow classical liquid is given by

$$v^2 = \left(\frac{f\lambda}{2\pi} + \frac{2\pi\sigma_t}{\rho\lambda}\right) \tanh\left(\frac{2\pi d}{\lambda}\right) \tag{3}$$

where f is the restoring force per unit mass at the surface, λ is the wavelength, σ_t is the surface tension, ρ is the density, and d is the depth of the liquid. In our case, the wavelength is long compared to the film thickness so the surface tension term is negligible. The restoring force is the van der Waals attraction that the substrate exerts on the helium. The expression becomes

$$c_3 = \sqrt{\frac{\rho_s}{\rho} a_{\mathrm{vdW}} d} \tag{4}$$

where a_{vdW} is the van der Waals acceleration and d is the film thickness. The factor $\frac{\rho_s}{\rho}$ is necessary as only the superfluid component is in motion. The magnitude of the van der Waals attraction is a function of both the material and condition of the surface.

Initial attempts to describe attenuation of third sound waves consider several dissipative mechanisms. Since only the normal component of a superfluid carries heat, third sound—motion of only the superfluid component—is also a temperature wave, with higher temperature in the troughs of the wave (greater normal density) and lower temperature in the crests (lower normal density). As a result, helium evaporates at the troughs and re-condenses at the crests, dissipating energy. Heat transfer through the substrate and the vapor is also dissipative. The evaporation/re-condensation mechanism is implicitly included in the solution for complex third sound velocity by Atkins.[10] This approach is further developed by Bergman.[11, 12] In thick films, heat transfer through the substrate and the vapor, as well as the effects of vapor confinement[15–17] can be neglected, and the evaporation/re-condensation (Atkins/Bergman) mechanism is expected to be the dominant cause of dissipation. As mentioned, however, these models give values for attenuation much smaller than observed and cannot account for the history dependence of observed attenuation. Ellis and co-workers[6, 18] have modeled the films as inhomogeneous, filled with trapped vortices—the presence of which might account for the unexpectedly high attenuation in thick films and the observed irreproducibility of

measurements. Ellis[6] suggests that the attenuation may be caused by vortex drag along the substrate surface. Penanen and Packard[14] propose a mechanism where mutual friction between the vortex cores and the normal component, and viscous drag experienced by the vortex dimple at the free surface, are responsible for the attenuation.

Since attenuation due to vortices should depend on the film thickness, our initial goal was to determine attenuation α as a function of film thickness d. Due to the large history dependent variation in attenuation that was apparent in films of the same thickness, however, it became clear that a systematic determination of $\alpha(d)$ was beyond the scope of this experiment. Therefore all the results reported here are derived from a single film thickness of ~ 30 nm.

3. SYSTEM AND METHOD

We perform our experiments in an open circular resonator, shown schematically in Fig. 1. We use electrodes to capacitively excite and detect the third sound waves.[19] The base of the resonator is a cylindrical brass pedestal with a diamond-milled top (experimental) surface. AFM images of the diamond-milled surface indicate surface RMS roughness of approximately 15 nm (see Appendix A). A turret shaped spacer is screwed onto the pedestal, supporting a glass optical flat, which serves as the upper surface of the resonator. Supporting the glass by the edges avoids capillary filling of the space between the brass substrate and the glass optical flat. Gold electrodes are evaporated onto the glass, with four excitation/detection quadrants of area $\sim 1.63\,\mathrm{cm}^2$ each, separated by a grounding cross to reduce capacitive cross-talk (see pattern in Fig. 1). Before evaporating the electrode pattern, eight small pieces of gold foil are glued to the glass to provide robust electrical contact to the quadrants and grounding cross. Electrical connections are made using spring contacts, which are inserted in epoxy pods in the turret and press into the gold foil pads. The separation between the surfaces of the resonator is adjusted by placing Kapton® or aluminum spacers either between the pedestal and the turret or between the turret and the glass flat. The separation is measured capacitively and is found to be between 38 and 60 μm for each quadrant. During the experiments, saturated films of helium cover the brass pedestal and glass flat. Since the surfaces are of different diameters, each has a distinct set of resonances.

The resonator assembly is surrounded by a cylindrical capacitive helium level meter and placed inside a sealed brass can. The can is thermally connected to the cold stage of a single-shot ^{3}He adsorption refrigerator via a thin copper wire. The temperature is measured by a germanium

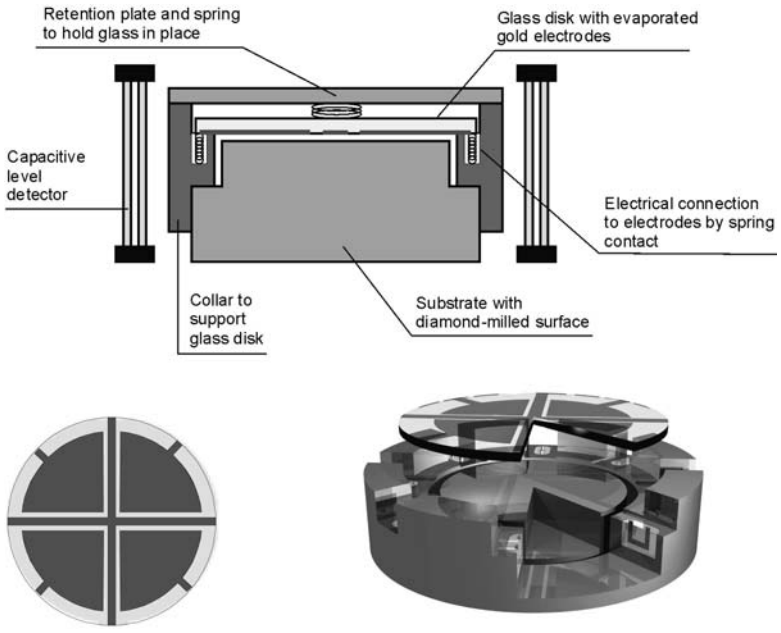

Fig. 1. Top: Schematic of resonator. Bottom left: Pattern of gold electrode evaporated on glass optical blank, including four excitation/detection quadrants and a grounding cross to reduce capacitive cross-talk. Electrical contact is made via springs pressing into gold pads at the periphery of the glass. Bottom right: Resonator assembly.

resistance thermometer and is controlled by a commercial feedback system and a metal film resistor used as a heater. The observed temperature stability is better than 0.1 mK between 0.29 and 2.2 K. Lack of temperature stability would lead to broadening of the resonances, discussed in the results section. The temperature stability does not eliminate the possibility of temperature gradients in the experimental cell, the possible effects of which we will also discuss.

We use a homemade superfluid-tight ^{3}He-actuated valve with closing pressure of approximately 300 psi. This prevents helium vapor reflux in the fill capillary. Reflux of the film, if permitted to occur, results in a marked decrease in cryostat performance (both base temperature and hold time). It also causes thermal gradients inside the cell, which affect the film properties. The valve is placed just above the cell and, after closing and evacuation, eliminates any thermal link to the cell through the fill capillary.

Hold time of the ^{3}He refrigerator ranges from 5 to 30 hours, depending on the temperature of the cell. Re-condensation of the ^{3}He to prepare for another run requires cycling the cell up or down in temperature to

1.5 K, as the re-condensation process thermally links the cell to the 1 K pot. Unless otherwise specified, "run" or "cool-down" refers to a single condensation of the ^{3}He.

When collecting data, the substrate and grounding cross are electrically grounded. The typical value of the capacitance between each of the electrode quadrants and the substrate is 38 pf. The polarizability of the liquid (helium has a dielectric constant $\varepsilon \approx 1.055$) means a voltage applied to one of the quadrants draws helium into that part of the capacitor. An oscillating voltage at the appropriate frequency can thus excite a resonant mode in the helium film. The dielectric nature of helium also makes it possible to detect the resonance capacitively; a change in the amount of dielectric material between the substrate and one of the quadrants results in a change in capacitance.

We determine the attenuation from the width of third sound resonances. We use two techniques to measure these resonances, continuous wave (CW) and pulsed (see circuit schematic in Fig. 2). For the CW method, we apply an oscillating voltage, typically less than 1 V, at frequency f, to one of the electrode quadrants. Since the force on the film is proportional to the square of the applied voltage, the resonant response is at frequency $2f$. We detect the oscillations in film thickness on another quadrant, either adjacent or diagonally opposite to the excitation quadrant. We use a constant-charge bias detection scheme, which gives higher sensitivity than that of capacitance bridge technique at the relevant frequencies (see Appendix B). The signal is then amplified by a low-noise pre-amplifier, and the $2f$ component of the output is detected with a lock-in amplifier. Once the resonance is allowed to ring up, both the in- and out-of-phase signals are recorded as a function of f. The response is modeled as the complex sum of resonances in the helium films on both surfaces and of the relative motion of the capacitor plates. Since the third sound velocities in our

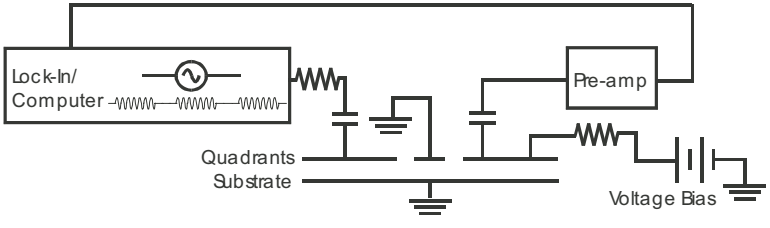

Fig. 2. A schematic of the third sound generation and detection electronics. For the continuous wave method, the reference output of the lock-in amplifier provides the excitation signal. For the pulsed method, excitation bursts are applied with a computer-controlled digital-to-analog converter.

experimental regime are on the order of 1 m/s and the substrate radii are roughly 2 cm, typical response frequencies are tens of Hertz.

In the pulsed method, an excitation burst at a frequency near resonance, typically tens of volts RMS amplitude and several cycles in duration, is applied to one of the electrodes. The signal from the detection quadrant, either adjacent or opposite to the excitation quadrant, is recorded digitally and Fourier analyzed to extract the resonant response. To improve the signal-to-noise ratio, a series of (~ 10) pulses is averaged before the Fourier transform is performed. Though averaging improves signal-to-noise significantly, experimental evidence indicates that the excitation burst itself is sufficient to alter the properties of the film, and the averaging may be masking these effects. Non-linear response of the film makes quality factor and attenuation values extracted from a single pulse measurement dependent on the drive pulse amplitude. The reported quality factor and attenuation values are from measurements made in the linear regime, unless indicated otherwise.

Extracting the quality factors and attenuation values from the response data requires an understanding of the excitation spectrum. The mode structure can be described well by two sets of Bessel function modes of a drum head, one in the film covering the brass substrate and the other in the film on the glass surface (see model of spectra in Fig. 3). In the continuous method, there is an additional term due to the mechanical flexing of the capacitor plates. This term is present in an empty cell; it is smooth in the frequency range of interest, and is subtracted in the analysis. The solution of the wave equation for a cylindrical geometry gives the wave height h as a function of position,

$$h_{mn}(r, \phi, t) = J_m(k_{mn} r) \cos(m\phi)\, e^{i\omega_{mn} t} \tag{5}$$

where J_m is the cylindrical Bessel function of order m, k_{mn} is the wave number determined by application of boundary conditions, and ω_{mn} is the angular frequency.

We assume that the thickness oscillation of the film goes to zero at the edges of the substrate and glass. This boundary condition corresponds to the tangential component of the local velocity field vanishing at the edge, eliminating the need for vorticity at the edge. This gives the dispersion relation

$$\omega_{mn} = c_3 k_{mn} = \frac{c_3 Z_{mn}}{R}, \tag{6}$$

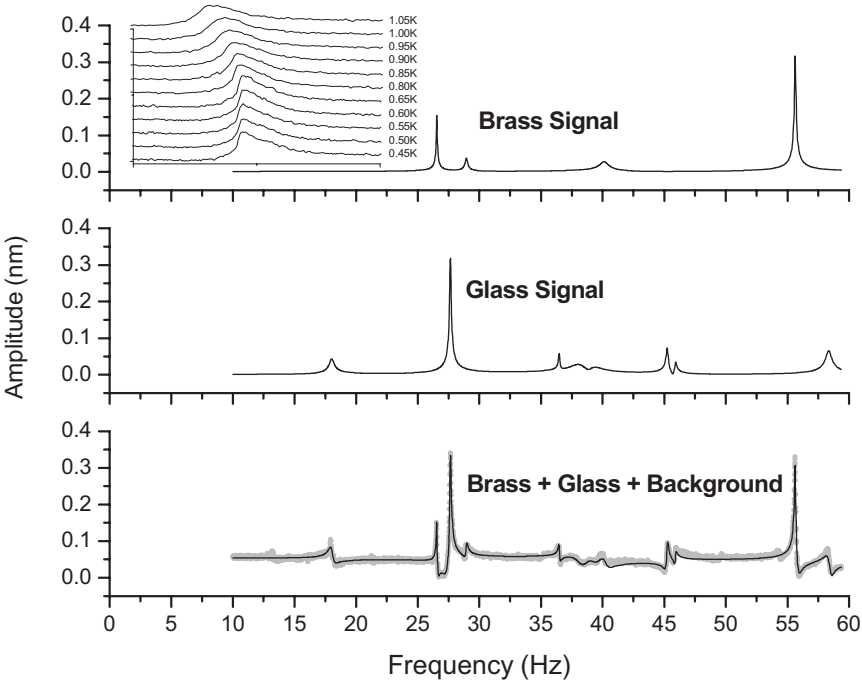

Fig. 3. Top and middle: Model of the film response on each surface, the brass substrate and the glass flat with gold electrodes. Bottom: The composite signal includes the response from both the glass and brass substrates as well as a background signal due to relative motion of the two surfaces. The response is a function of drive voltage frequency. The model signal is overlaid on a measured film response at a single temperature. Inset: Measured temperature dependence of strongest signal, the (1, 1) mode on the glass surface, near 28 Hz.

with c_3 the speed of third sound, R the radius of the surface in question, and Z_{mn} the nth zero of the Bessel function of order m, i.e., $J_m(Z_{mn}) = 0$. For example, the first two zeros of J_0 are 2.405 and 5.520.

We are able to identify the first several resonant features in the spectrum, which correspond closely to the predicted features with the boundary conditions described above. One check of the correspondence is the ratio of the frequencies of the features. The ratio of the frequency of the first two modes on each surface, (0, 1) and (1, 1), is expected to be equal to the ratio of the Bessel zeros, $\frac{Z_{11}}{Z_{01}} = \frac{3.832}{2.405} = 1.593$. For the data shown in Fig. 3, the ratios are 1.512 and 1.535 for the brass and glass surfaces, respectively. Most of the measurements were performed on the (1, 1) anti-symmetric mode on the glass surface which is most efficiently excited by the electrode geometry described above.

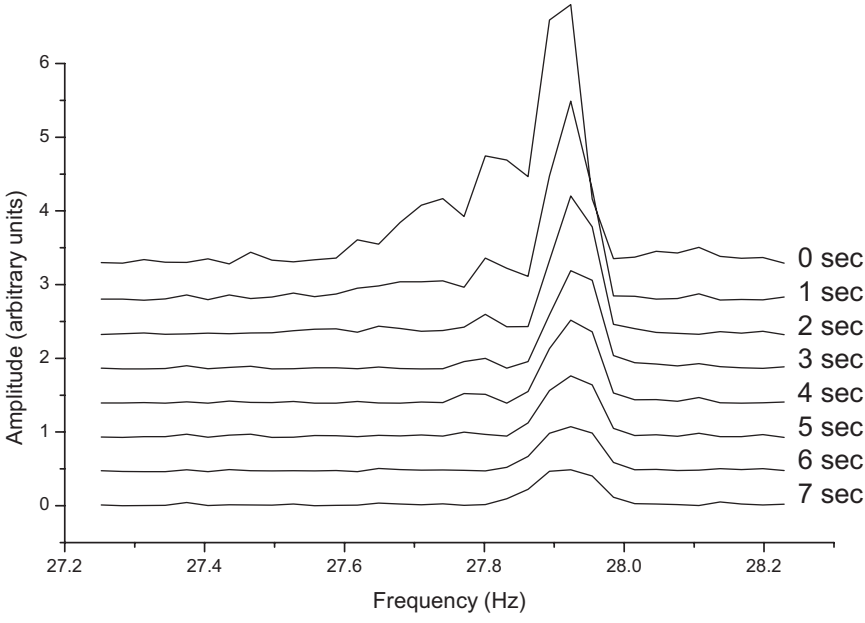

Fig. 4. Pulsed method data analysis illustration. A series of FFT power spectra of the same real-time signal are shown with 0–7 s delay between excitation pulse and data collection. The broader features decay more quickly, and the main resonant mode can be analyzed with a simple Lorentzian model.

When using the CW method, the quality factor can be extracted by fitting the measured response to the described model for the response spectrum. In the pulsed method, accurate analysis requires that the nearby modes have significantly lower quality factors than the mode being studied. If the real time signal is acquired after the response of nearby modes has decayed, the resonant curve is very nearly Lorentzian and then analysis is straightforward. This is illustrated in Fig. 4, which shows the power spectrum obtained by Fourier transforming the response with varying intervals of delay from the start of the signal ("dead" time). The feature with shorter time constant decays away, leaving a more symmetric central feature. Note that similar asymmetric or non-Lorentzian behavior would be observed if the mode in question shows non-linear behavior at higher amplitudes. Such non-linearity can be detected by comparing response to pulses of different amplitudes.

The quality factors Q, determined from the fits of the resonant response, and the attenuation α are related via

$$\alpha = \frac{\omega}{2Qc_3} \tag{7}$$

In a resonator where the reflection at the boundary is imperfect, the attenuation can be presented as:

$$\alpha_{\text{measured}} = \alpha_{\text{boundary}} + \alpha_{\text{3rd}} \tag{8}$$

The energy loss α_{boundary} is due to partial transmission of the wave at the boundary. At sufficiently low temperatures where $\rho_s \cong \rho$, the transmitted component should be temperature independent. On the other hand, the intrinsic third sound attenuation is expected to vanish as temperature is lowered. Thus, one would expect to be able to infer the intrinsic third sound attenuation α_{3rd} by subtracting the low temperature limit from the measured values.

4. RESULTS

The results we report come from films of approximately 30 nm. Thickness is determined in two ways. In the first method, we measure the change in capacitance of one of the quadrants at 300 mK before and after adding helium to the cell. This gives a value of 59.6 nm total thickness between the plates of the resonator, which we assume to be evenly divided between the gold (evaporated on glass) and brass surfaces, a reasonable assumption since the van der Waals potential is similar for brass and gold. Uncertainties in film thickness values calculated in this manner are due to possible capillary condensation on the rough surfaces and possible change in capacitance of the coaxial wires within the cell.

Film thickness can also be calculated from the height of the substrate above the bulk level of helium and the van der Waals attraction of the helium to the substrate. There is disagreement over the exact value of the van der Waals attraction of a polished metal substrate, perhaps due to uncertainties of surface quality. Reported values[20–22] determined experimentally for the van der Waals attraction of a polished metal substrate predict a film thickness of 33–47 nm.

4.1. Third Sound Attenuation and Mode Frequency as a Function of Temperature

Figure 5 shows attenuation as a function of temperature for sets of measurements from two different cool-downs on a single film of the (1, 1) mode. As noted previously, between sets of measurements, the film warms/cools to approximately 1.5 K as the ^{3}He re-condenses. Attenuation decreases monotonically as temperature decreased down to roughly 0.8 K. A significant feature of the data set is that the scatter in values at a given temperature

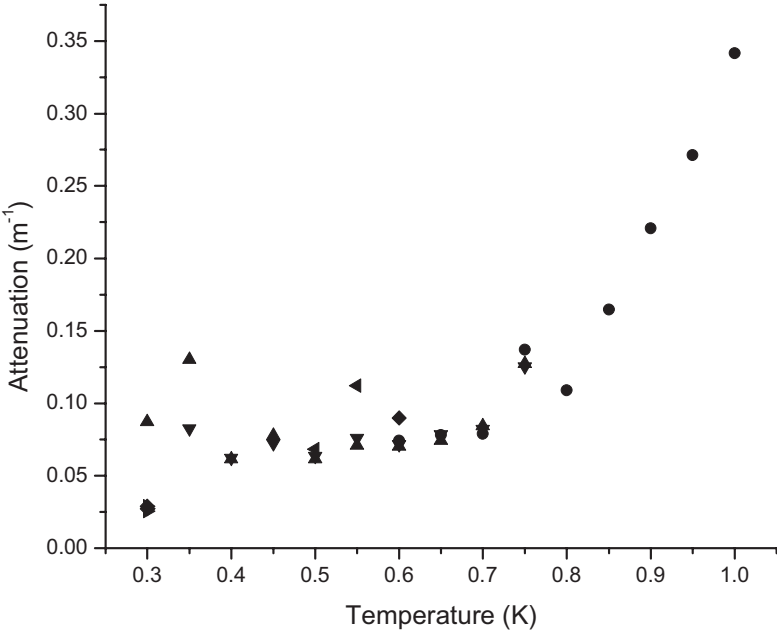

Fig. 5. Attenuation of the (1, 1) mode as a function of temperature for several cool-downs (represented by different symbols). Error bars are smaller than the symbol size on this scale and are not shown.

is much greater than the uncertainty in any single measurement. This implies that the attenuation is not intrinsic to the film, depending instead on some change in the structure of the film. The values we measure for attenuation are considerably smaller than those measured previously,[2] though previous measurements are for frequencies above 100 Hz.

The minimum value of the measured attenuation for a single film, generally reached near $T = 0.7$ K, varies from cool-down to cool-down (cycles of the ^{3}He system). From analysis given previously (see Eq. (8)), we would expect the attenuation to reach some saturation value at low temperatures, an effect which is not apparent in the data.

The position of the (1, 1) resonance as a function of temperature is presented in the inset of Fig. 6. In the absence of sudden temperature changes (more than approximately milli-Kelvin per second) the resonant frequency is a smooth decreasing function of increasing temperature. The position of the resonance is a function of both film thickness and superfluid density. Since the thickness of a saturated film is not dependent on temperature, the temperature dependence of the position of the resonance is expected to be the same as the temperature dependence the superfluid

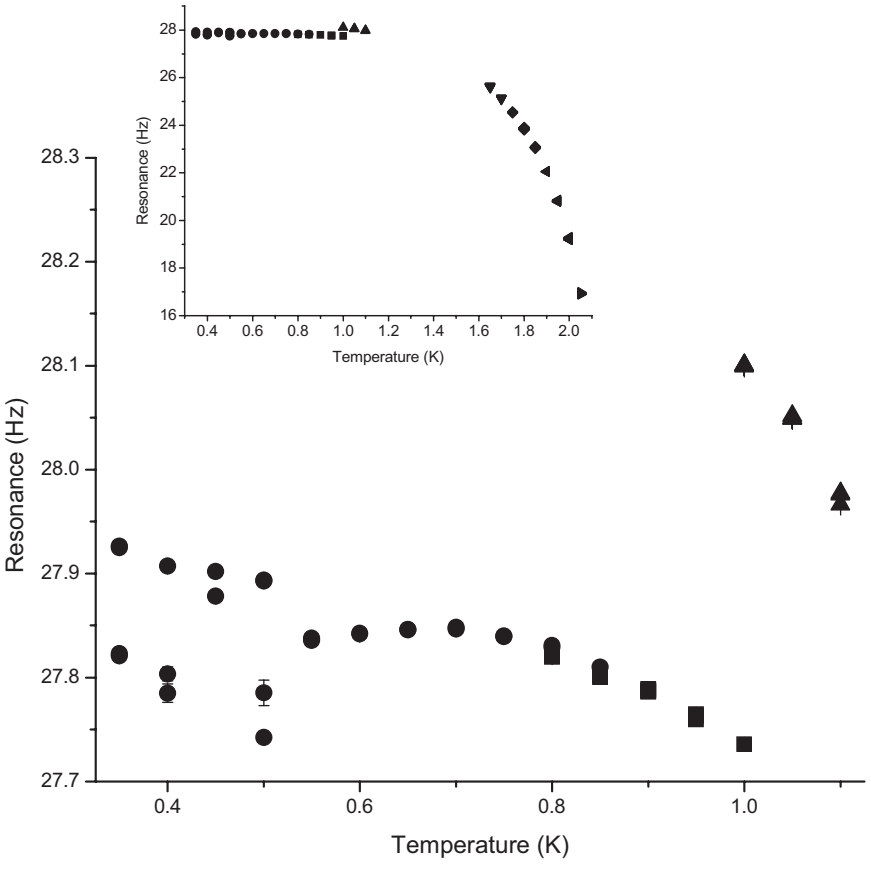

Fig. 6. Inset: Resonant frequency of the (1, 1) mode as a function of temperature. Main graph: Detail of low temperature portion of inset. Error bars are considerably smaller than the scatter. Different symbols denote data taken during different cool-downs.

density in the film, ρ_s. If the cell is disturbed, as is the case when the ^{3}He refrigerator is cycled, we observe small but discernable shifts in the resonance frequency (see main portion of Fig. 6). The superfluid-tight valve remained closed throughout these measurements.

4.2. Non-Linearity and Hysteresis

As drive amplitude is increased, third sound resonances measured by the CW method exhibited non-linear behavior such as hysteresis (Fig. 7) and deviation from the low-amplitude shape (Fig. 8). Since the van der Waals attractive potential acceleration is a rapidly decreasing function of

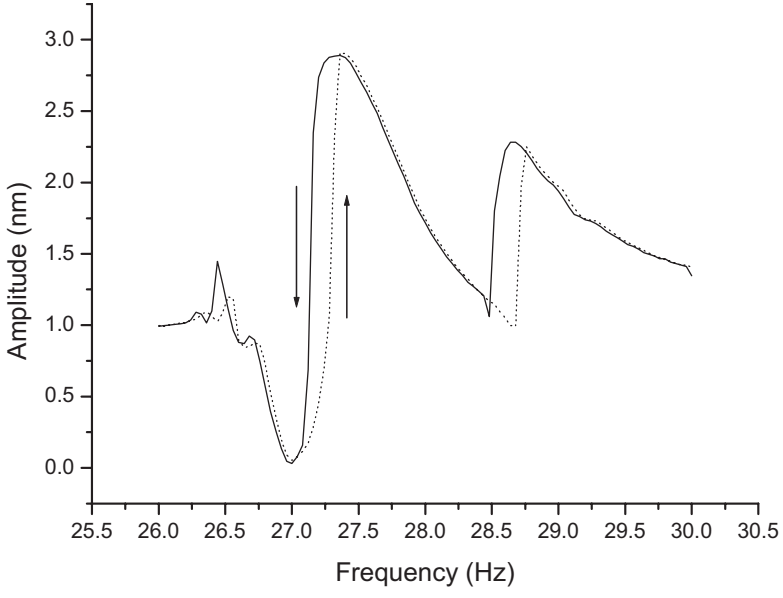

Fig. 7. Hysteresis in high-amplitude third sound, 95 V RMS drive. The data is taken with increasing (solid) and decreasing (dotted) frequency. Since the van der Waals attractive potential is a strong function of film thickness, such non-linear behavior is expected when the thickness variation is a substantial fraction of the equilibrium film thickness.

distance from the surface, the local speed of the third sound speed is higher in the troughs and lower on the crests. In addition, in the CW method, the average value of the square of the drive field introduces an additional term in the chemical potential, making the film thicker on average, which shifts the resonant frequency downward. We can expect non-linear behavior when the response amplitude (height of third sound wave) becomes a significant fraction of the film thickness. Since our data fitting technique relies on the assumption that we are studying a linear oscillator, we must avoid the nonlinear regime. To allow for meaningful interpretation of attenuation data, the response in the studied films (i.e., height of third sound wave) is kept to no more than 0.1 nm, less than one percent of the film thickness. However, even in this regime we see noticeable deviation from linear response when the shift down in frequency becomes comparable to the width of the response (see Fig. 8).

To verify that we were in the linear regime, we confirmed that the resonant response scales as the square of the excitation voltage. An example of this verification is shown in Fig. 9.

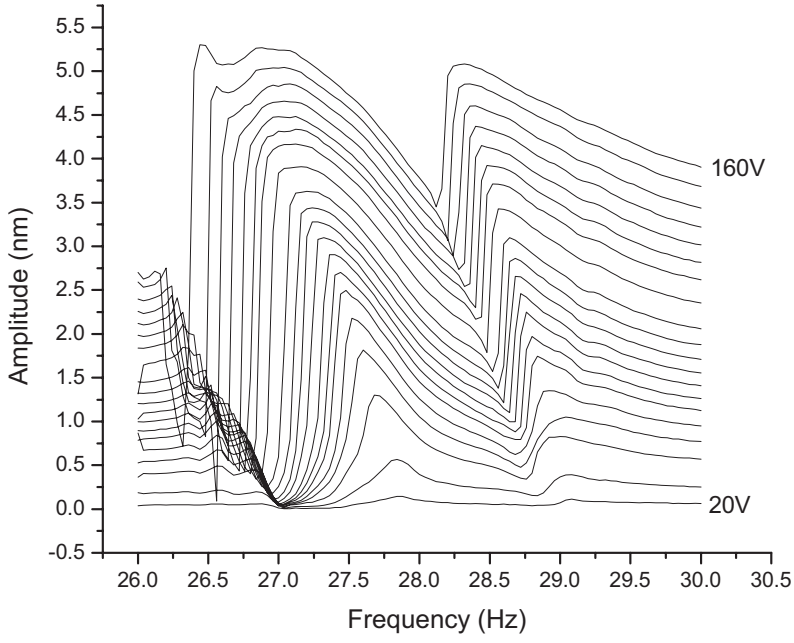

Fig. 8. A set of resonant curves at different drives (5 V increments) in the non-linear oscillator regime. As with hysteretic effects, such behavior is expected as a result of the significant variation in the van der Waals potential for wave amplitudes comparable to film thickness. Note also shift in downward in resonance frequency due to film thickness change. Distortion of linear response becomes apparent when frequency shifts are comparable to peak width. The data on attenuation was taken with drive voltage below 5 V.

4.3. Temperature Changes, Ramps, and Spikes

It is possible that temperature gradients in the film or transient variations in temperature might affect the film structure. These changes might show up in attenuation or mode frequency measurements. In order to explore the effect of unintentional thermal gradients in the cell, we took data while purposely creating such gradients, repeatedly cycling slowly between 0.4 and 0.425 K. The temperature was raised or lowered every 15 seconds by 0.25–1.25 mK, stretching the temperature ramp to cover the entire 5 to 25 minute data taking period. Since the cell heater is on the outer surface of the brass vacuum can, cooling the cell will leave the substrates, with the helium films we are probing, temporarily hotter than the outer cell. The resulting fountain pressure creates a thicker helium film on the substrate than would be present if the temperature were uniform. An increase in film thickness would be observable by a shift downward in the

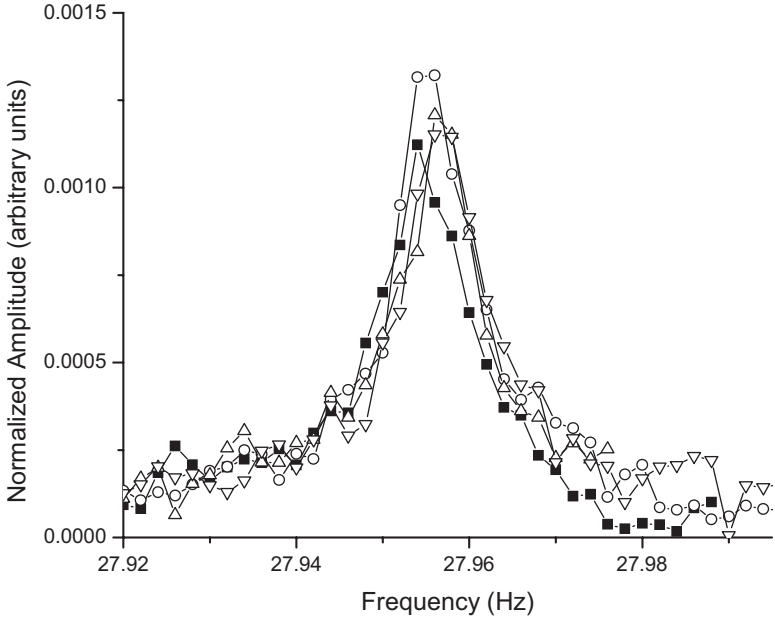

Fig. 9. Resonant response normalized to the square of drive amplitude for excitation drives of 1.25, 1.5, 1.75, and 2 Volts. The consistency of the plots verifies response in the linear regime.

resonant frequency. In Fig. 10, we show the resonant frequency and quality factors for a series of temperature ramps. Resonant frequencies were indeed depressed in measurements taken while temperature was slowly ramped down, indicating thickening of the film due to fountain pressure. In the same measurements, the measured quality factor does not exhibit a well-defined trend. Calculations using available data on helium entropy suggest that a temperature difference of 0.1 mK between the outer cell and the substrate would account for the observed shift in resonant frequency of roughly 5 mHz. If the ramp rates used in these measurements are characteristic of the typical temperature variation during a (nominally) stable-temperature attenuation measurement, the variation in film thickness would result in a broadening of the resonance curve. At typical frequencies for our measurements (25 Hz), this broadening would put a limiting value on the quality factor of $Q = \frac{f}{\Delta f} \approx 5000$, which corresponds to an attenuation α of 0.0225 m^{-1}.

In an attempt to understand the variation in attenuation between cool-downs of the ^{3}He refrigerator, we take a series of measurements after temperature spikes (large, rapid temperature excursions). Between each

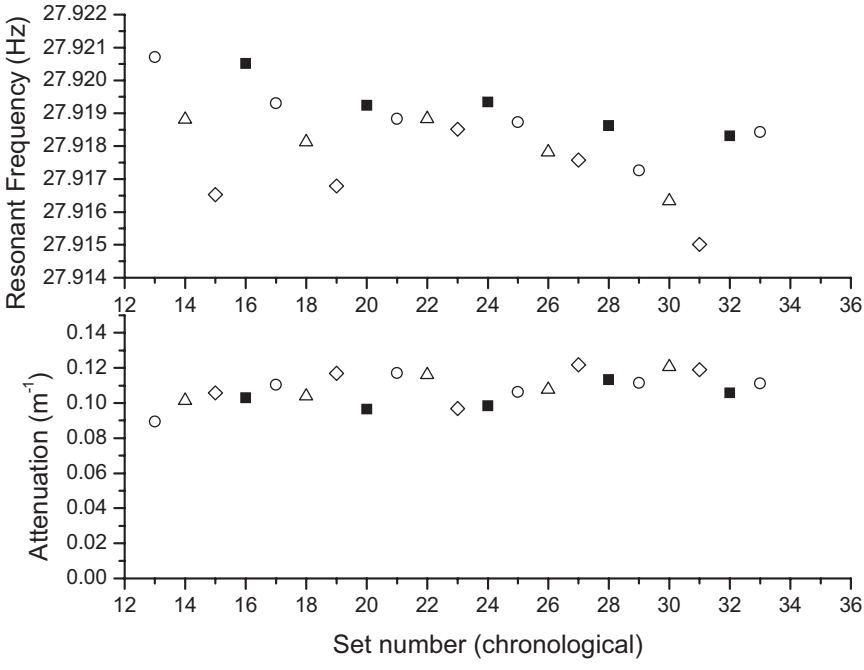

Fig. 10. Resonance frequency (top) and the quality factor (bottom) for a film undergoing heating and cooling. The resonant frequency exhibits discernable trend, with the lowest frequency during cooling (◇) and highest frequency when at stable lower temperature (■). We believe that the frequency shift is due to the film thickness change caused by fountain pressure if the temperature in the cell is not uniform. ■ are measurements taken at stable 400 mK, ○ are measurements during a steady warm-up to 425 mK, △ at 425 mK, and ◇ during a steady cool-down to 400 mK.

measurement shown in Fig. 11, the cell is warmed to approximately 1 K with a short (approximately 1 second) heat pulse. The cell is allowed to cool to 0.4 K and stabilize before a measurement is taken. The range in quality factors for these measurements is dramatically larger than after slow temperature ramps, with values differing by a factor of 2.5. Likewise, there is large scatter in the resonant frequencies, with shifts as large as 25 mHz. The variation in quality factors is much larger than the uncertainly in any single measurement. The correlation between the resonant frequency and the attenuation is weak.

4.4. Splitting of Resonant Modes

The resonant modes we study, including the azimuthally asymmetric (1, 1) mode we focus upon, can be represented as a superposition of

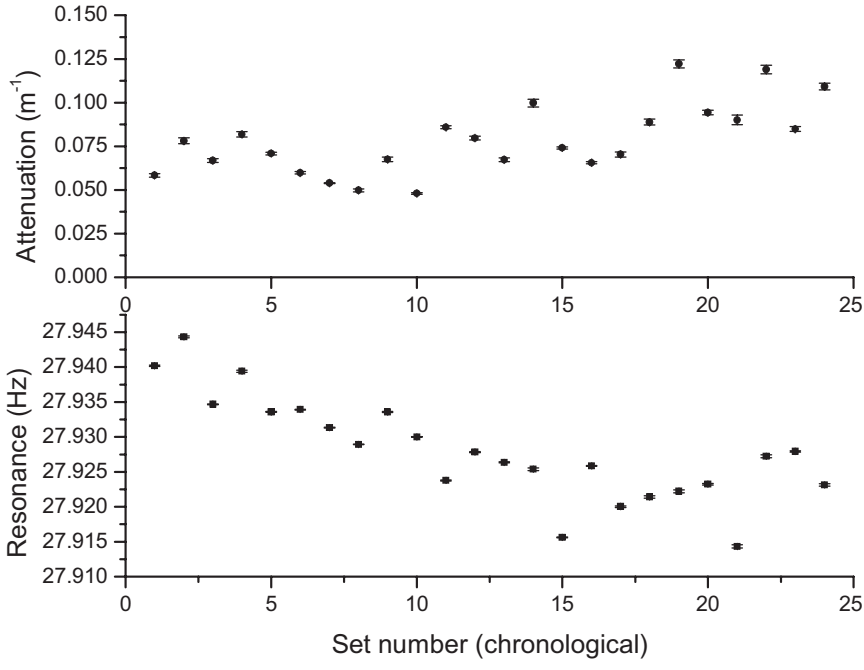

Fig. 11. Attenuation and resonance peak positions for a set of measurements at 400 mK. A heat pulse bringing the cell to ~ 1 K is applied between the measurements, after which the cell temperature is allowed to equilibrate. Attenuation scatter, which is considerably larger than the error bars for an individual measurement, is much larger than in measurements shown in Fig. 5, for slow temperature ramps. Thus that data shows that large, sudden changes in temperature can alter the properties of the film.

frequency-degenerate traveling modes, one propagating clockwise, the other counter-clockwise. At temperatures below ~ 0.4 K, several modes exhibit frequency splitting (Fig. 12). The existence and magnitude of the splitting is variable (shown in Fig. 13), affected by both large temperature excursions (such as re-condensation of ^{3}He in the adsorption refrigerator) and mechanical disturbances (for example, tapping on the dewar). In the absence of such thermal or mechanical perturbation, the splitting remains stable during a run of up to 30 hours.

One explanation for the lifting of the degeneracy of these modes is a deviation of the resonator shape from circular; however, the fact that the magnitude of the frequency splitting varies indicates that this is not the case. Other plausible explanations are variation of the boundary conditions along the periphery of the circular films or trapped net vorticity in the film.[18, 23, 24] Trapped net vorticity would mean that the circular film contains

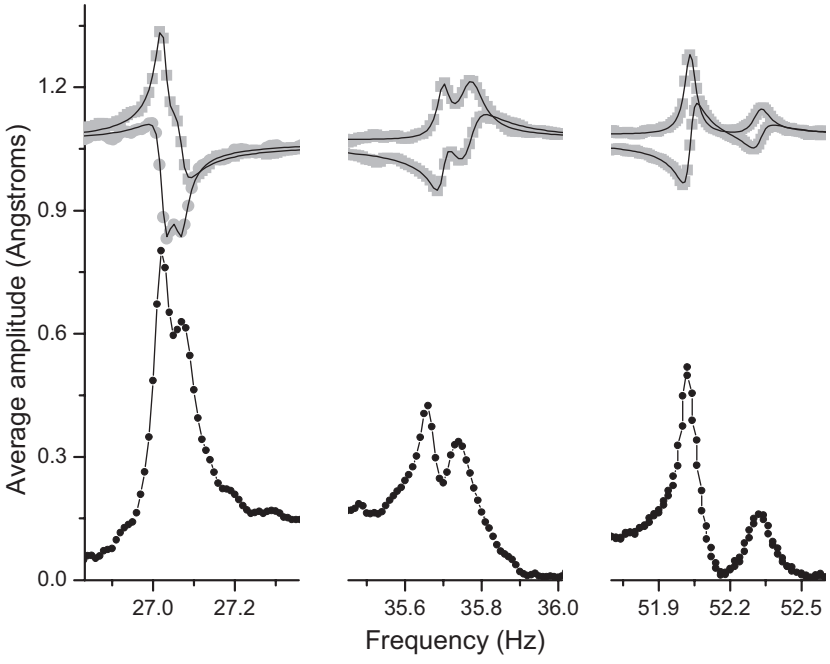

Fig. 12. Splitting of the (1, 1), (1, 2), and (1, 3) modes on the glass surface measured at 310 mK, 8 V drive. The inset illustrates in-phase and quadrature components fit with two peaks for each mode.

net circulation. This would result in a Doppler shift of the otherwise degenerate modes up and down in frequency relative to each other.

The magnitude of frequency splitting for different modes is not expected to be the same for a given film with trapped circulation,[24] as it is a function of the position of the radial maximum of the azimuthal velocity of the wave. If the vortex distribution were uniform, however, one would expect the magnitude of splitting to either increase or decrease for both modes between runs; in fact we observe that in some cases the splitting increases for one mode and decreases for the other. A possible interpretation is a non-uniform distribution of vortices in the film.

4.5. Speed of T_λ Traversal

If vortex formation is driven by supercritical helium flow, the amount of trapped vorticity may be influenced by the rate at which the superfluid transition is traversed. We attempted to investigate this by measuring attenuation after warming above 2.17 K, then cooling at different rates.

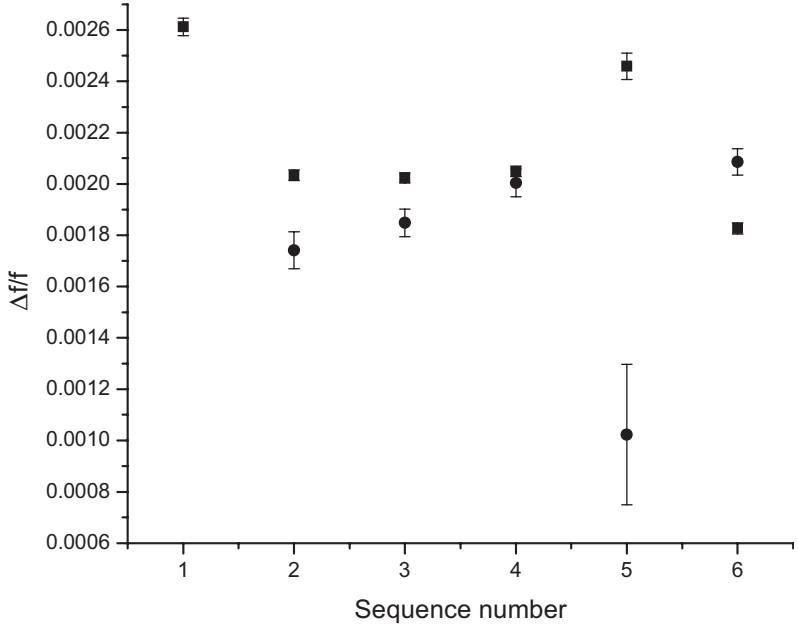

Fig. 13. Magnitude of frequency splitting of the (1, 1) (squares) and (1, 2) modes (circles) induced by mechanical disturbance of the refrigerator. Frequency splitting is not constant from cool-down to cool-down, indicating that degeneracy is lifted not due to geometric asymmetries but rather to either changes in boundary conditions or net trapped vorticity. Inconsistent direction of change of different modes from run to run may be indicative of non-uniform vortex distribution.

The cell temperature is stabilized at $T \sim 2.19$ K, above the superfluid transition. The average heater power necessary to keep temperature constant is recorded. The heater power is then set to a lower value, so that the difference would determine the effective cooling power. We observed no systematic effect of varying the time of cooling from 2.19 to 2.165 K from several minutes to several hours (see Fig. 14). Note that any heat pulse to the system, including the measurement itself, may reset the state.

5. DISCUSSION AND CONCLUSION

If the superfluid film were defect homogeneous and defect-free, one would expect measurements of the attenuation to be reproducible. The attenuation values (and to a lesser extent the resonant frequencies) measured in this work and in previously reported third sound data do not exhibit such simplicity. The observed variations in attenuation and frequency for nominally identical thermodynamic conditions are significant.

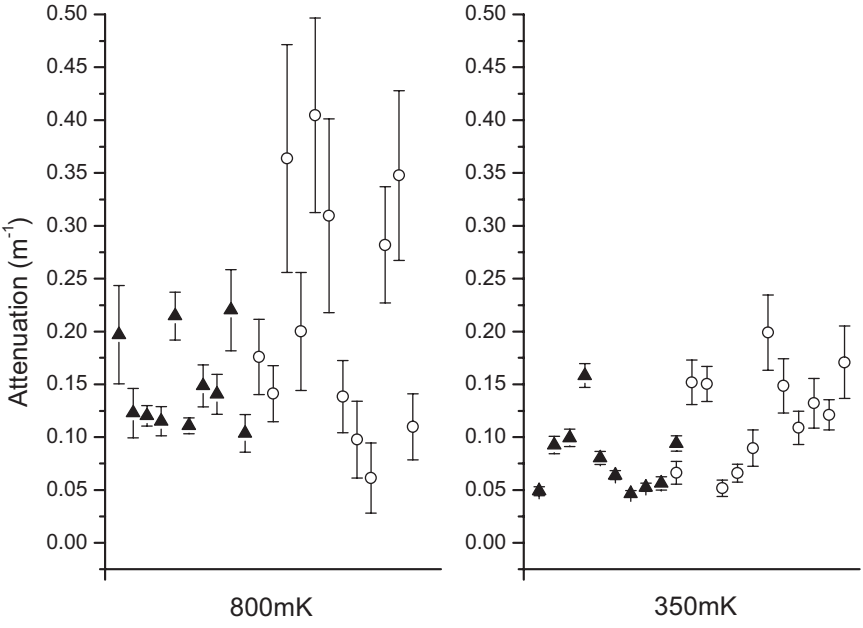

Fig. 14. Comparison of attenuation for multiple data points taken after two different crossings of T_λ. Closed triangles represent controlled crossing over several hours, open circles uncontrolled crossing over several minutes. No systematic difference is observed.

It seems that a valid interpretation of the data implies a metastable structure or property within the film that can be changed by temperature sweeps and mechanical perturbation.

One possible model consistent with observed behavior is that presented Penanen and Packard.[14] In that model, the third sound attenuation in the films is to be due to remnant quantized vortices. The energy loss is mostly due to the drag experienced by the vortex dimples at the free surface of the film moving through clamped normal component. Such dissipation, unlike in vortex drag and tangle/reconnection models, is linear in oscillation amplitude.

We performed a check of dissipation linearity by Fourier analyzing the same pulsed response with variable pause time after the excitation pulse, as illustrated in Figs. 15 and 16. Thus, we are able to measure the quality factor as a function of third sound amplitude. Within the error bars of the measurement, the quality factor is independent of third sound amplitude, as long as the response remains Lorentzian (i.e., is within the linear excitation regime). In vortex drag and vortex re-connection mechanisms,[6] the attenuation is a faster-than-linear function of wave amplitude. In this case,

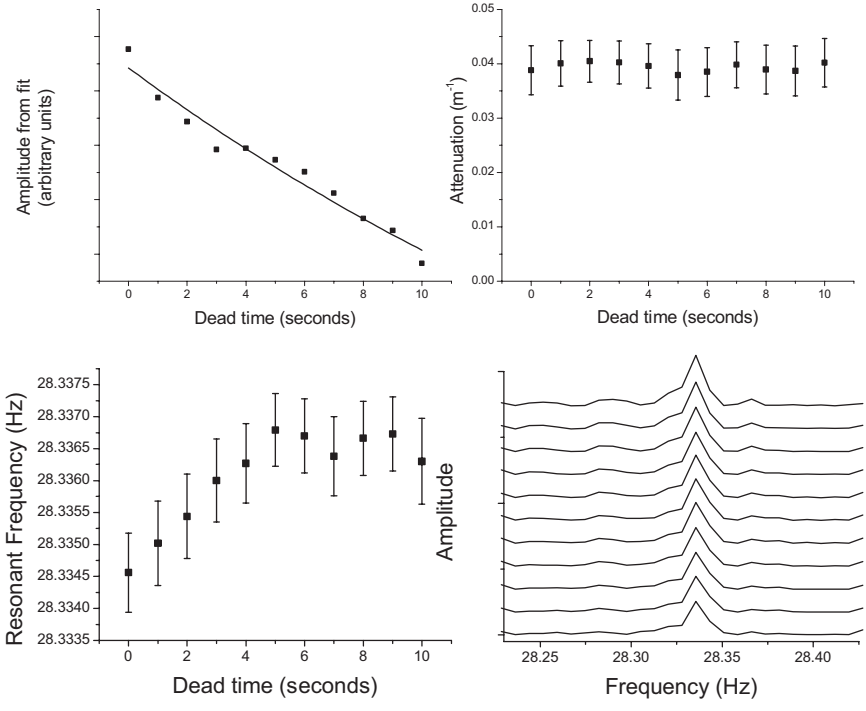

Fig. 15. A single measurement of a third sound resonance decay measured by pulsed method at 300 mK. The fitted amplitude, attenuation and the resonance frequency are plotted as a function of dead time (the pause between the end of the excitation pulse and the beginning acquisition of the real-time signal for FFT). The signal exhibits exponential decay. Within experimental error, quality factor is independent of response amplitude, suggesting a linear attenuation mechanism.

the lack of temperature dependence is also interpreted as an indication of re-connection mechanisms dominating the attenuation. While our experiments cannot rule out such explanation, our observations seem to be consistent with a linear attenuation mechanism—vortex dimple drag and incomplete reflection being two possibilities.

Alteration of vortex population, either increase or decrease, could be explained by rapid temperature changes. Thermally driven superfluid flow could create or remove vortices. Such change may not have a significant effect on the total density of trapped vortices, but could conceivably significantly alter the net vorticity in the cell. This would result in trapped circulation and manifest itself via mode splitting, as observed here and elsewhere.[18, 23, 24] In our measurements the net vortex density consistent with the observed spitting is on the order of $10^5\,\mathrm{cm}^{-2}$, identical to the density theorized by Ellis.[24]

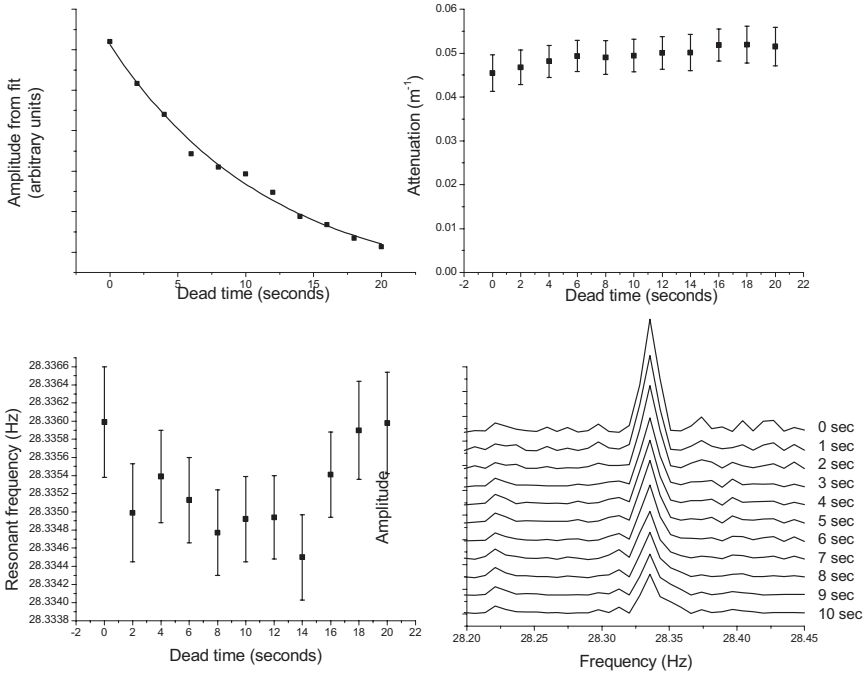

Fig. 16. Analysis of a single pulse measurement following the pulse shown in Fig. 15. A higher attenuation is observed, but the decay remains exponential and magnitude of attenuation remains independent of response amplitude.

An attenuation mechanism dependent on the total vortex density also provides an explanation for the observed lack of reproducibility between cool-downs, as the density may vary with each traversal of T_λ. The observed values of attenuation allow us to make a rough estimate of the total vortex density in the films. Based on the model of Penanen and Packard,[14] we find a density of approximately $10^{13}\,\mathrm{cm}^{-2}$. Such a vortex density could easily have net density fluctuations on order of the $10^5\,\mathrm{cm}^{-2}$ indicated by observed mode splitting.

An anonymous referee suggested that flow at the film boundary should be considered as the cause of the observed attenuation. Fixed boundary conditions (see Sec. 3) leave the velocity field finite at the substrate edge. Dissipation in this flow, possibly due to vortices bound or generated at the edge, may then exhibit the hysteresis and the temperature dependence described in this manuscript. Since the film is thicker at the concave boundary, the attenuation could be stronger there.

As shown in Eq. (8), dissipation dominated by incomplete reflection from the boundary would be expected to reach a constant, limiting value at

low temperature, which is not seen in Fig. 5. Note also that the scatter in attenuation values in Fig. 5 is a result of crossing the superfluid transition. Since the amount of helium in the cell is such that the film remains saturated well above the transition temperature, we deem it unlikely that the capillary condensation profile (and thus the boundary conditions) change as a result of such temperature excursions. This would not rule out attenuation due to vortices trapped at the boundary only. Impedance to radial flow at the boundary can be expected to modify the boundary conditions and change the mode structure. There is, however, close correspondence of the modes to the predicted frequency response (see previous discussion of the ratio of the Bessel zeros) for fixed boundary conditions.

Finally, higher than expected attenuation of third sound has been observed in time-of-flight experiments,[25] where boundary effects do not play a role. Additional evidence that trapped vorticity, whether at the boundary or on the substrate proper can be seen in experiments on films with small ^{3}He impurity concentrations.[26]

In summary, we find evidence that thick films of superfluid ^{4}He contain substantial populations of metastable vortices. Future work with such systems should be done with an eye toward controlling surface and temperature effects that may substantially affect such a population and thus alter measurements of properties such as attenuation.

APPENDIX A. SUBSTRATE PREPARATION

The resonator surface of the brass substrate was diamond-milled in the mechanical engineering department of UC Berkeley. The surface was analyzed under an atomic force microscope. Looking at a 20 μm square patch of the brass, the surface exhibited RMS roughness of approximately 15 nm and peak-to-peak roughness of approximately 120 nm.

APPENDIX B. CHOICE OF DETECTION METHOD

The signal-to-noise ratio in the experiments we describe is limited by several factors, related to both excitation and detection. For excitation, increasing the applied voltage will correspondingly increase the signal and is mostly limited by the requirement that the film be kept in a linear response regime.

The measurement frequency range and the electrode capacitance determine the most suitable method for third sound detection. One option is to use a double lock-in detection scheme. In this case, third sound is excited by applying a signal to one of the electrodes (drive electrode). The other electrode (detection electrode) is part of a capacitance bridge

operated at a higher frequency (~ 2000 Hz). The bandwidth of the detection lock-in amplifier is set to ~ 200 Hz. The output of the detection lock-in amplifier is measured by the drive lock-in amplifier at the second harmonic. The amplitude of the detection drive is limited due to heat dissipation; we observe noticeable cell heating (almost 2 mK) with 5 V bridge excitation. The heating is likely to be due to the charging current in the electrodes and electrode contacts. This heating scales linearly in frequency, as expected. Local film heating, although not seen by the thermometer mounted outside the cell, may still substantially alter the film behavior via fountain pressure effects. This mechanism may be relevant in other reported experiments,[27] where the detection electrode was a part of a resonant circuit with excitation frequency on the order of 20 kHz.

An alternative detection technique, used in the experiments we report here, is a constant charge bias scheme. The detection electrode is charged to 122 V through a large resistor R (1 GΩ). The time constant for charging, RC, is on the order of 1 s, where C is the sum of the electrode and coaxial cable capacitances (~ 1 nF). The electrode then acts as a capacitive "microphone" and is connected to a low-noise preamplifier through a large capacitor. This detector operates in constant charge regime, and the amplitude of the signal on the preamplifier is proportional to the rate of capacitance change. The output of the preamplifier is detected by the lock-in amplifier at the second harmonic of the drive frequency. At approximately 10 Hz, one can reasonabley expect a factor of 7.5 improvement in the signal-to-noise over the double lock-in scheme.

APPENDIX C. $\frac{TS}{L}$ CORRECTION TO SUPERFLUID DENSITY

Equation (4) shows that that velocity of a third sound wave (or frequency of a third sound resonance) should be proportional to the square root of the superfluid fraction. In fact, there is an additional factor of $(1+\frac{TS}{L})$ predicted by Bergman,[11,12] where T is the temperature, S is the entropy, and L is the latent heat of vaporization. This correction is usually neglected, as the second term in the parenthesis is very small everywhere except very near T_λ. Additionally, previously reported values for third sound velocity near T_λ have been smaller than predicted by theory[2] and have been analyzed in the context of Atkins[2,10] prediction of a weaker correction to the superfluid density of $\sqrt{1+\frac{TS}{L}}$.

In Fig. 17, we compare the resonant frequency as a function of temperature to the square root of the superfluid density and with and without the $\frac{TS}{L}$ corrections. The data does seem to suggest that a modification to the superfluid density is necessary.

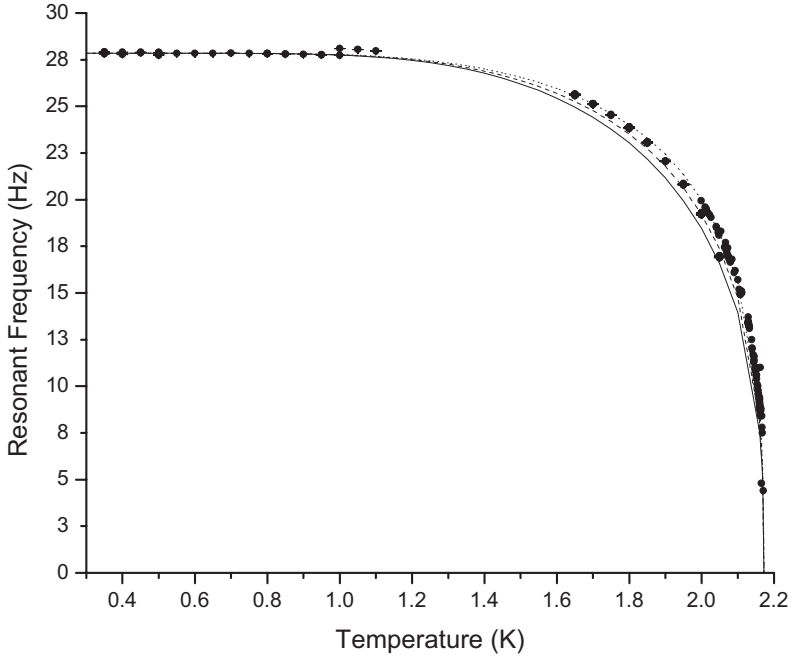

Fig. 17. Comparison of measured resonance frequency of third sound (filled circles) to $\sqrt{\frac{\rho_s}{\rho}}$ (solid line), $\sqrt{\frac{\rho_s}{\rho}(1+\frac{TS}{L})}$ (dashed line), and $\sqrt{\frac{\rho_s}{\rho}}(1+\frac{TS}{L})$ (dotted line).

ACKNOWLEDGMENTS

We would like to acknowledge Prof. F. M. Ellis for his early work and theories regarding vorticity in superfluid ^{4}He. This work was supported by the NSF and NASA.

REFERENCES

1. C. W. F. Everitt, K. R. Atkins, and A. Denenstein, *Phys. Rev. Lett.* **8**, 161 (1962).
2. C. W. F. Everitt, K. R. Atkins, and A. Denenstein, *Phys. Rev.* **136**, A1494 (1964).
3. I. Rudnick, R. S. Kagiwada, J. C. Fraser, and E. Guyon, *Phys. Rev. Lett.* **20**, 430 (1968).
4. T. G. Wang and I. Rudnick, *B. Am. Phys. Soc.* **17** (1972).
5. K. Telschow and R. B. Hallock, *B. Am. Phys. Soc.* **29**, 699 (1975).
6. F. M. Ellis and H. Luo, *Physica B* **169**, 521 (1991).
7. A. M. R. Schechter , R. W. Simmonds, R. E. Packard, and J. C. Davis, *Nature* **396**, 554 (1998).
8. P. A. Sheldon and R. B. Hallock, *Phys. Rev. B* **50**, 16082 (1994).
9. D. T. Eckholm and R. B. Hallock, *Phys. Rev. B* **21**, 3913 (1980).
10. K. R. Atkins, *Phys. Rev.* **113**, 962 (1959).
11. D. Bergman, *Phys. Rev.* **188**, 370 (1969).
12. D. Bergman, *Phys. Rev. A* **3**, 2058 (1971).

13. S. J. Putterman, R. Finkelstein and I. Rudnick, *Phys. Rev. Lett.* **27**, 1697 (1971); M. Chester and R. Maynard, *Phys. Rev. Lett.* **29**, 628, (1972); Both theories were rebuked in M. W. Cole and D. L. Goodstein, *Phys. Rev. A* **9**, 2806 (1974).
14. K. Penanen and R. E. Packard, *J. Low Temp. Phys.* **128**, 25 (2002).
15. H. van Beelen and G. Bannink, *Physica B* **121**, 30 (1983).
16. H. van Beelen and G. Bannink, *Physica B & C* **122**, 151 (1983).
17. G. Bannink, M. G. M. Brocken, I. Vanadel, and H. Van Beelen, *Physica B & C* **115**, 376 (1983).
18. F. M. Ellis, L. Keeler, and C. Wilson, *Physica B* **194-196**, 673 (1994).
19. J. S. Brooks, F. M. Ellis, and R. B. Hallock, *B. Am. Phys. Soc.* **23**, 49 (1978).
20. W. E. Keller, *Phys. Rev. Lett.* **24**, 569 (1970).
21. R. B. Hallock and E. B. Flint, *Phys. Rev. A* **10**, 1285 (1974).
22. G. A. Williams and R. E. Packard, *Phys. Rev. Lett.* **32**, 587 (1974).
23. F. M. Ellis and H. Luo, *Phys. Rev. B* **39**, 2703 (1989).
24. F. M. Ellis and L. Li, *Phys. Rev. Lett.* **71**, 1577 (1993).
25. T. G. Wang and I. Rudnick, *J. Low Temp. Phys.* **9**, 425 (1972).
26. K. Penanen, J. A. Hoffmann, J. C. Davis, and R. E. Packard, *J. Low Temp. Phys.* **134**, 1069 (2004).
27. F. M. Ellis and R. B. Hallock, *Rev. Sci. Instrum.* **54**, 751 (1983).